Article

Impact of Homogenization Treatment on the Microstructure, Recrystallization and Mechanical Behavior of Hot-Rolled Mg-Al-Zn-Ca Alloy

Rajesh Kannan Arasapan , Hafiz Muhammad Rehan Tariq , Muhammad Ishtiaq , Ha-Seong Baek , Umer Masood Chaudhry , Tea-Sung Jun *

Posted Date: 30 September 2025

doi: 10.20944/preprints202509.2423.v1

Keywords: Mg alloy; homogenization treatment; texture; mechanical properties; particle stimulated nucleation (PSN)

 doi:10.20944/preprints202509.2423.v1

Article

Impact of Homogenization Treatment on the Microstructure, Recrystallization and Mechanical Behavior of Hot-Rolled Mg-Al-Zn-Ca Alloy

Rajesh Kannan Arasapan [1,2], Hafiz Muhammad Rehan Tariq [1], Muhammad Ishtiaq [3], Ha-Seong Baek [1], Umer Masood Chaudhry [1] and Tea-Sung Jun [1,2,*]

[1] Department of Mechanical Engineering, Incheon National University, Incheon, 22012, Republic of Korea

[2] Research Institute for Engineering and Technology, Incheon National University, Incheon 22012, Republic of Korea

[3] Department of Materials Engineering and Convergence Technology, Gyeongsang National University, Jinju 52828, Republic of Korea

* Correspondence: t.jun@inu.ac.kr

Abstract

The present study systematically investigates the effect of homogenization treatment on the microstructural evolution, recrystallization behavior, and mechanical response of a hot-rolled Mg-3Al-1Zn-1Ca alloy. Detailed microstructural characterization revealed that Al2Ca precipitates were uniformly distributed along grain boundaries in the as-received (AR) condition, where they contributed to significant pinning of boundary migration. Homogenization treatment (350 °C, furnace cooling) resulted in non-uniform grain coarsening, driven by the interplay of precipitate pinning and differential stored strain energy, while also facilitating particle-stimulated nucleation (PSN) and recrystallization. Electron backscatter diffraction (EBSD) analysis confirmed a substantial increase in the fraction of high-angle grain boundaries and recrystallized grains in the heat-treated (HT) state, with kernel average misorientation (KAM) and grain orientation spread (GOS) analyses indicating pronounced recovery of lattice distortions. Mechanical testing demonstrated a significant decrease in yield strength (263 MPa to 187.4 MPa) and hardness (65.7 to 54.1 HV) due to dislocation annihilation and stress relaxation, while ultimate tensile strength remained nearly unchanged (~338 MPa) and ductility improved markedly (12.6% to 16.4%). These findings highlight the dual role of Al2Ca precipitates in promoting recrystallization through PSN while simultaneously restricting excessive grain growth through Zener pinning.

Keywords: Mg alloy; homogenization treatment; texture; mechanical properties; particle stimulated nucleation (PSN)

1. Introduction

Magnesium (Mg) alloys are gaining attention in the transportation industry for their potential to reduce vehicle weight [1–4]. However, their widespread use faces challenges because, compared to other structural materials, Mg alloys have lower specific strength and show difficulties in formability and workability due to their hexagonal close-packed (HCP) crystal structure [5–7]. While Mg has multiple slip systems, high critical resolved shear stress (CRSS) values hinder effective activation, leaving only basal slip systems operational at room temperature [8,9]. This inadequacy in uniform deformation is compensated for by twins, which accommodate plastic strain during deformation [10,11].

The AZ series of Mg alloys stands out as the most prevalent and economically viable option among commercially available Mg alloys. As outlined in the Mg-aluminum (Mg-Al) binary phase diagram [12], the equilibrium β-phase constitutes second-phase precipitates, characterized by

 doi:10.20944/preprints202509.2423.v1

$Mg_{17}Al_{12}$. These secondary phase particles exert varying effects on microstructure and texture evolution throughout thermomechanical processing, with their impact depending upon factors like size and distribution within the material [1,13]. However, the β-phase is intrinsically brittle and thermally unstable, often accelerating crack initiation and limiting ductility during service. To overcome these challenges, alloying strategies have been explored to suppress the formation of β-$Mg_{17}Al_{12}$ and instead promote the development of more stable intermetallic compounds. Rare-earth (RE) additions have been shown to effectively refine grains, weaken basal textures, and enhance ductility by consuming Al and forming Al-RE phases [14]. Nonetheless, the high cost and limited supply of RE elements restrict their application in large-scale production. Calcium (Ca) has emerged as a cost-effective alternative, reacting with Al to form thermally stable Al_2Ca particles that impede dislocation motion and grain boundary migration, while also reducing reliance on β-$Mg_{17}Al_{12}$ [15]. During hot rolling, these Ca-containing precipitates alter the CRSS by elevating the resistance to basal slip and twin propagation while facilitating non-basal slip activity. Although this shift in deformation mechanisms helps to weaken basal texture, the rolling process still introduces significant strain heterogeneity and internal stresses into the microstructure. To stabilize the beneficial effects of Ca additions and further optimize the balance between strength and ductility, post-deformation annealing becomes essential. This process relieves internal stresses, modifies the microstructure, and enhances precipitation strengthening. For instance, Chaudry et al. reported that annealing of as-rolled AZ61-CaO alloys promoted the formation of $(Mg, Al)_2Ca$ precipitates, suppressed twinning, and significantly improved the tensile strength through precipitation hardening [16]. In Mg-Al-Zn alloys containing secondary phases, annealing after thermomechanical processing has also been shown to accelerate particle-stimulated nucleation (PSN), facilitating recrystallization and reducing the dominance of basal textures, which in turn leads to more randomized grain orientations and improved formability [17].

So far, systematic studies on the microstructural and mechanical response of Mg–Al–Zn–Ca alloys subjected to heat treatment remain limited. Therefore, it is essential to investigate how annealing influences the particle distribution, texture development, and deformation behavior of such alloys. In this work, a Mg-3Al-1Zn-1Ca (by wt.%) alloy plate produced by hot rolling was examined in both as-received and heat-treated conditions. Detailed microstructural characterization was performed to analyze the morphology, fraction, and crystallographic features of intermetallic phases. Microhardness and tensile testing were conducted to evaluate the mechanical response. This comprehensive approach enables a deeper understanding of the interplay between heat treatment, microstructure, and mechanical properties in Mg-Al-Zn-Ca alloys.

2. Materials and Methods

A 1 mm thick Mg-3Al-1Zn-1Ca alloy plate, produced by hot rolling, was obtained from POSCO, South Korea. The alloy was further heat-treated at 350 °C, followed by furnace cooling. For microstructural analysis of both the as-received (AR) and heat-treated (HT) specimens, samples were sectioned into 10 mm × 5 mm pieces from the rolling direction-transverse direction (RD-TD) plane. The specimens were cold-mounted to preserve structural integrity, then subjected to the standard metallographic preparation procedure mentioned elsewhere [18]. To characterize the distribution and morphology of intermetallic particles, scanning electron microscopy (SEM, JSM-7800F, JEOL) equipped with energy-dispersive X-ray spectroscopy (EDS) was employed. The particle fraction in the AR specimen was quantified using ImageJ software. Microstructure and texture evolution of the AR and HT specimens were further investigated using electron backscatter diffraction (EBSD) in an SEM (SU-500, Hitachi) equipped with an EBSD system (Velocity™ Super, EDAX). EBSD scans were performed over an area of 300 μm × 300 μm with a step size of 0.5 μm, and the data were analyzed using OIM 8.6 software.

Microhardness measurements were carried out at 10 different points on the RD-TD plane using a micro-Vickers hardness tester under a 1.96 N load and 5 s dwell time. For tensile testing, dog bone-shaped specimens were prepared from the hot-rolled sheets via water jet cutting, following ASTM

 doi:10.20944/preprints202509.2423.v1

E8 standard dimensions, with a thickness of 1 mm and a gauge length of 25 mm. Tests were conducted at room temperature (~24 °C) using a universal testing machine (UTM, RB 301 UNITECH-T, R&B) at a strain rate of 1×10^{-3} s^{-1}. An axial extensometer (3542 model, Epsilon Tech.) was attached to the gauge section to record strain accurately.

3. Results

3.1. Influence of Homogenization Treatment on Microstructure and Texture Modification

Figure 1 presents a comparative analysis of phase composition and its distribution in the hot-rolled Mg-Al-Zn-Ca alloy.

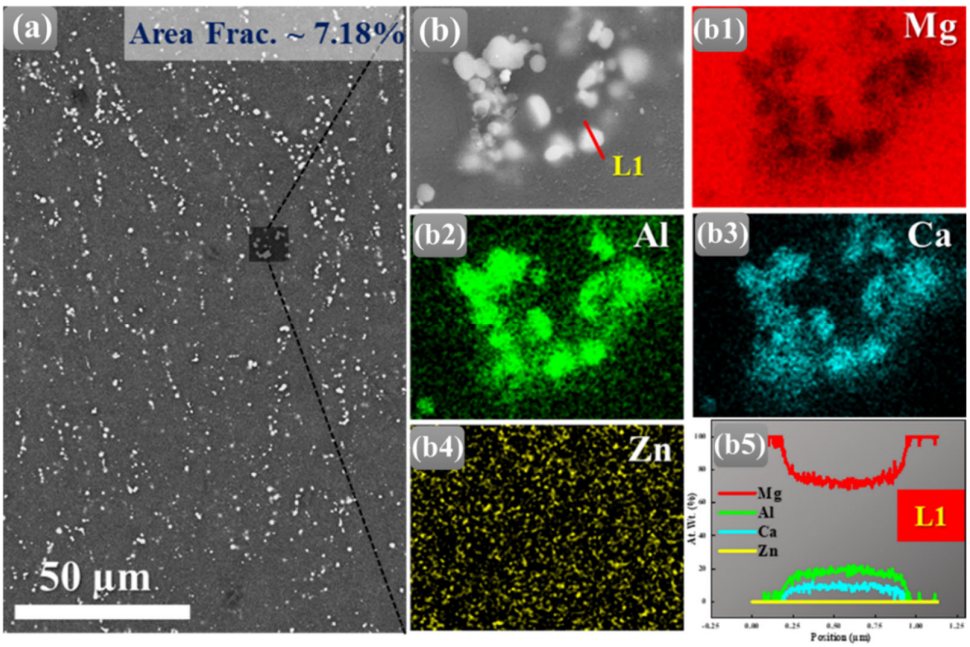

Figure 1. SEM micrographs and EDS analysis of secondary phase particles in the Mg-Al-Zn-Ca alloy: (a) BSE image showing the distribution of second-phase particles. (b) Magnified SEM images of the selected regions in (a), highlighting the morphology of the particles. (b1-b4) Corresponding EDS elemental mapping of Mg, Al, Ca, and Zn, showing enrichment of Al and Ca in the second-phase regions. (b5) EDS line-scan profiles (L1) across representative particles, confirming elemental segregation.

The backscattered electron (BSE) image (Figure 1a) shows bright contrast particles uniformly dispersed in the Mg matrix with an area fraction of ~7.18%, while the magnified view (Figure 1b) highlights their irregular morphology, typical of solidification-induced segregationEDS elemental mapping (Figures 1 (b1-b4)) highlights significant enrichment of Al and Ca in the particles with corresponding depletion of Mg, whereas Zn remains relatively uniform in the matrix, indicating limited participation in the secondary phases. This clearly indicates the role of Zn as a solid solution-strengthening element rather than a constituent of the secondary phases. The EDS line scan across a representative particle (Figure 1 (b5)) further confirms compositional segregation, with distinct peaks of Al and Ca and a dip in Mg, supporting the identification of Al-Ca-rich intermetallics such as Al_2Ca or $(Mg, Al)_2Ca$, which are widely reported in the literature as stable, high-melting compounds [19,20]. The Al_2Ca intermetallic phase in Mg alloys is predominantly aligned along the basal plane of the α-Mg matrix [21]. This orientation is due to the crystallographic compatibility between the Al_2Ca phase and the α-Mg matrix, facilitating coherent precipitation [22].

These intermetallics are known to preferentially form at grain boundaries, enhancing creep resistance and thermal stability in Mg alloys, while Zn is generally retained in solid solution or forms Mg-Zn phases at higher contents [23]. The higher concentration of Ca and Mg reveals the formation

 doi:10.20944/preprints202509.2423.v1

of the Al_2Ca intermetallic phase, which consumes Al solute from the Mg matrix. Given that the atomic radius of Al (1.43 Å) is smaller than that of Mg (1.60 Å), the reduction in Al content results in a decrease in the average atomic size within the matrix. This reduction in atomic size causes the Mg lattice to expand, a phenomenon known as lattice dilation [24]. This lattice expansion can influence the alloy's mechanical properties by affecting dislocation movement and solid solution strengthening mechanisms.

Figure 2 shows the effect of homogenization treatment on the microstructure and texture evolution. The inverse pole figure (IPF) maps presented in Figures 2a and 2b clearly demonstrate that the average grain size increased from 6.3 μm in the AR sample to 10.4 μm in the HT sample. This increase in grain size is attributed to thermally driven grain growth during annealing, which is primarily governed by the reduction of grain boundary energy. However, the observed coarsening is non-uniform, as evidenced by the simultaneous presence of relatively coarse grains alongside fine grains. Such heterogeneous grain growth arises from variations in grain boundary mobility that are strongly influenced by precipitate pinning effects.

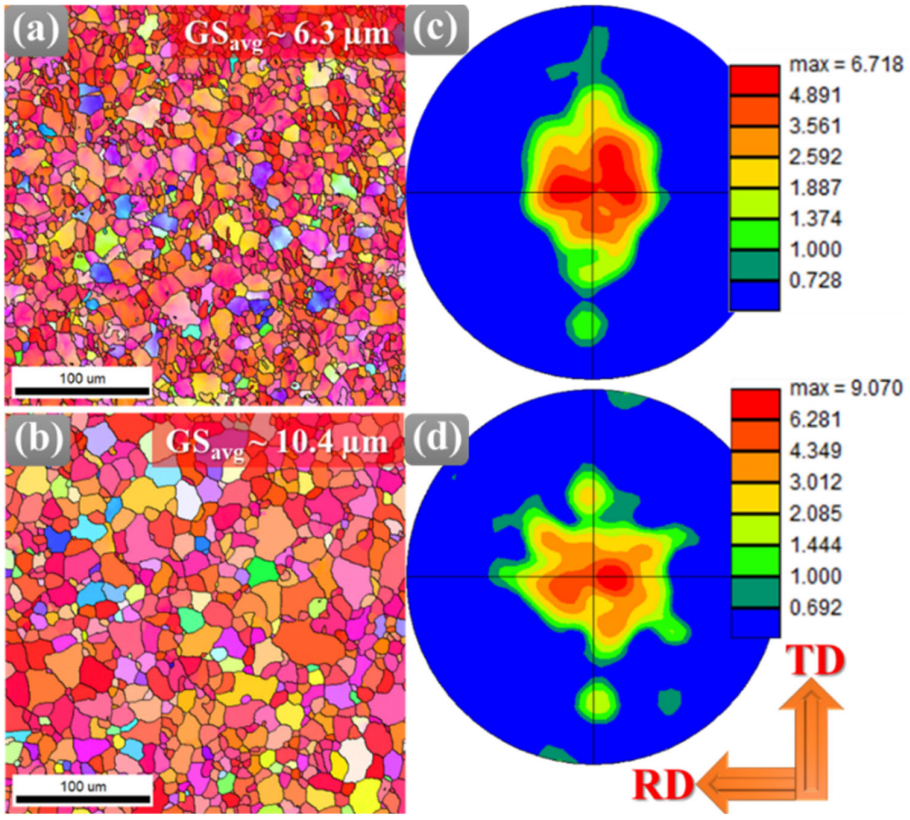

Figure 2. EBSD analysis showing **(a, b)** inverse pole figure (IPF) maps and corresponding **(c, d)** (0001) pole figures of the Mg-Al-Zn-Ca alloy in AR state and after HT, respectively.

The Al_2Ca precipitate tends to segregate at grain boundaries, exerting a retarding force on the boundary migration. Consequently, some grain boundaries remain stabilized, retaining a fine-grained morphology, whereas boundaries having lesser precipitate interactions migrate more freely, allowing abnormal growth of certain grains [25]. In addition, the heterogeneity in stored dislocation energy from prior hot-rolling deformation promotes differential growth rates, where grains with higher stored energy preferentially expand during annealing. As a result, the overall microstructure of the HT sample reflects an increase in average grain size but with significant inhomogeneity, characterized by the coexistence of abnormally large grains embedded within a finer-grained matrix.

It is well known that when particles are sufficiently coarse and well-spaced, particle-stimulated nucleation can dominate, leading to enhanced recrystallization [26]. The PSN mechanism greatly

 doi:10.20944/preprints202509.2423.v1

affects the texture evolution, which can be clearly observed from PFs shown in Figures 2c and 2d for AR and HT samples, respectively. For instance, the HT sample showed a dominant basal texture with a maximum intensity of ~9.1 m.r.d, higher than in the AR condition (~6.7 m.r.d.). Despite this maximum texture intensity, weaker texture components are observed surrounding the main basal orientation (Figure 2d). These secondary components likely originate from PSN near non-shearable Al_2Ca precipitates, where newly recrystallized grains adopt more random orientations, and from minor rotations of grains during grain growth. Thus, the HT sample demonstrates that extensive recrystallization can coexist with texture strengthening when orientation-selective grain growth dominates.

3.2. Impact of Homogenization Treatment on Recrystallization and Mechanical Behavior

Further magnified EBSD analysis has been performed on the HT specimen by acquiring a 50 μm × 50 μm map with a 0.02 step size to have a clear understanding of precipitate-grain boundary interaction on the recrystallization mechanism in a very localized area in detail (Figure 3). As Al_2Ca has an FCC phase and α-Mg has an HCP phase, the partitioning has been made based on the phase for the detailed orientation analysis. It can be seen clearly from the image quality (IQ) maps that brighter particles are distributed along the grain boundaries instead of the grain matrix (Figure 3a). Moreover, the grains surrounded by a higher fraction of these precipitates are smaller compared to the ones having fewer precipitates at their grain boundaries (Figure 3b). Further phase map in Figure 3c confirmed the FCC phase nature of Al_2Ca precipitates and the HCP phase nature of α-Mg. The precipitate-rich zones are further magnified in Figure 3 (c1). Each grain and precipitate orientation are also marked.

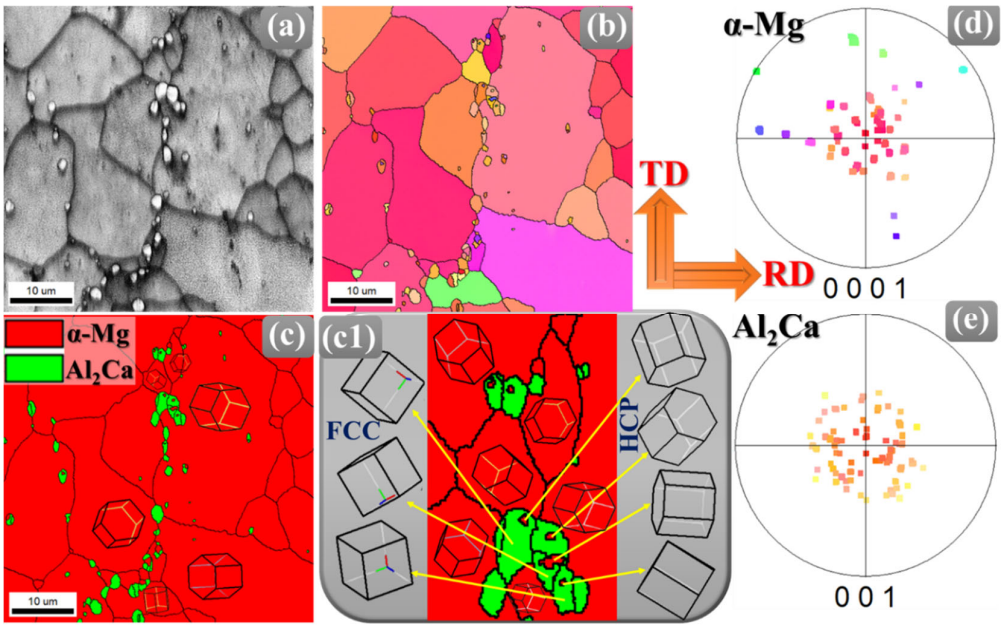

Figure 3. (a) IQ map, **(b)** IPF map and **(c)** phase map of the HT sample. **(c1)** Magnified region from (c) showing various α-Mg and Al_2Ca phases orientations. Discrete pole figures of **(d)** α-Mg and **(e)** Al_2Ca precipitates are derived from (b).

A detailed examination of the precipitate-matrix interface in the HT sample, as shown in the magnified phase map of Figure 3(c1), provides key insight into the precipitation mechanism in the annealed sample. The schematic representation of the unit cells reveals a well-defined crystallographic orientation relationship between the FCC Al_2Ca precipitates and the surrounding HCP α-Mg grains, indicating non-random interfacial alignment. This alignment minimizes interfacial

 doi:10.20944/preprints202509.2423.v1

free energy and enhances atomic coherency across the boundary, providing a thermodynamic driving force that governs the preferential orientation of the two phases. Such a structured relationship is characteristic of heterogeneous nucleation, in which the existing crystallographic planes of α-Mg act as favorable sites for Al_2Ca precipitate settling. A closer analysis of the orientation behavior of the HCP α-Mg matrix and FCC Al_2Ca precipitates, as illustrated in Figure 3(d-e), reveals distinct crystallographic characteristics and alignment tendencies. In Figure 3d, the clustering of points near the basal poles indicates that most α-Mg grains maintain low-angle deviations from a primary texture component, consistent with limited intragranular misorientation. In contrast, the Al_2Ca precipitates have a markedly different set of orientation clusters, as shown in Figure 3(e). These clusters are not random but rather indicate that the FCC unit cells adopt specific orientation relationships relative to the surrounding HCP matrix. This confirms that Al_2Ca precipitates preferentially align along certain crystallographic directions of the α-Mg matrix, such as aligning FCC {111} planes with HCP basal {0001} planes, which minimizes interfacial energy and promotes atomic coherency. Nevertheless, regions adjacent to Al_2Ca precipitates display deviations from this primary basal texture.

These locally misoriented α-Mg grains arise from PSN, where strain fields around rigid particles generate new grains with orientations that are rotated relative to the bulk texture. The resulting high-angle boundaries (HAGBs) and weakly oriented grains contribute to a broader orientation distribution, manifested as dispersed points around the main basal pole or minor secondary clusters in the pole figure.

Consequently, while the majority of the matrix maintains favorable basal alignment, PSN by Al_2Ca precipitates introduces localized heterogeneity, which can influence both the microstructural evolution and the orientation of precipitates in these regions. Importantly, this microstructural interplay also influences recrystallization. Second-phase particles, in combination with solute additions, modify grain boundary energetics through solute drag effects while controlling the kinetics of precipitate formation [27]. They promote nucleation via PSN and hinder grain growth through Zener pinning during recrystallization at the same time [28]. The distribution and size of Al_2Ca particles generate localized deformation fields that facilitate new grain nucleation, while their pinning action limits excessive grain coarsening.

Recrystallization is widely recognized as a fundamental mechanism for relieving localized stresses, leading to the formation of a microstructure with markedly reduced internal strain [29]. To quantitatively assess this stress relaxation and the associated microstructural heterogeneity, kernel average misorientation (KAM) analysis was applied (Figure 4). This method determines misorientation angles between neighboring points and estimates dislocation density by examining the first nearest neighbors within a maximum angular deviation of 5°, thereby providing a direct measure of local lattice distortion [30]. Here, Figures 4a and 4b show KAM maps with average KAM values for AR and HT samples, respectively. Figure 4a shows the greater strain accumulations within the grain matrix, which are homogeneously distributed throughout the microstructure of the AR sample. The higher KAM value (~0.8°) in the AR sample further reflects the high dislocation density induced by the initial hot rolling process. During primary thermo-mechanical processing, such as rolling, dislocation interactions and entanglements promote the formation of low-angle grain boundaries (LAGBs), which manifest as networks of dislocation walls and cellular substructures within the grains. After annealing, these entangled dislocations are largely annihilated or rearranged during recrystallization, releasing stored strain energy, thus forming strain-free grains with the lowest KAM value (~0.3°).

 doi:10.20944/preprints202509.2423.v1

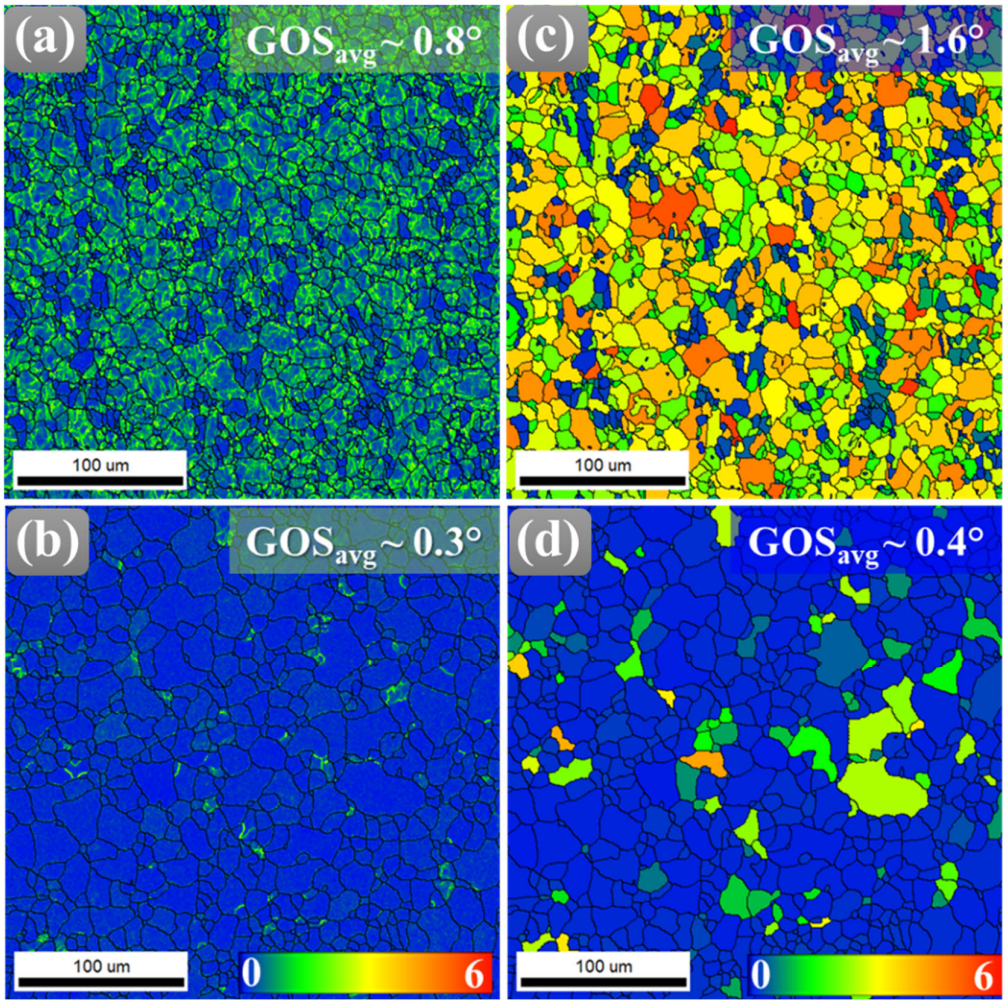

Figure 4. (a, b) grain orientation spread (GOS) maps, **(c, d)** kernel average misorientation (KAM) maps of the Mg-Al-Zn-Ca alloy in AR state and after HT, respectively.

Similarly, grain orientation spread (GOS) serves as a critical metric for quantifying intragranular misorientation uniformity. It directly reflects strain heterogeneity within grains and provides insight into the recovery mechanisms that reduce lattice distortion during annealing. In the AR sample, elevated GOS values arise from plastic strain accommodation, which generates complex dislocation substructures and pronounced lattice curvature. This results in a high average misorientation relative to the mean grain orientation. By contrast, the HT sample exhibits a pronounced reduction in GOS, as newly formed recrystallized grains possess nearly uniform internal orientations (Figure 4d). The transition from a high, non-uniform GOS distribution to a low, homogeneous one quantitatively demonstrates the replacement of deformed grains with strain-free counterparts, signifying the progression of recrystallization and the release of stored strain energy.

The role of Al_2Ca precipitates is particularly significant in this process. As thermally stable, non-shearable particles, they induce localized strain fields that hinder dislocation glide, promoting the accumulation and rearrangement of dislocations into LAGBs. During annealing, these LAGBs progressively absorb additional dislocations and rotate, transforming into HAGBs that define recrystallized grains [31,32]. The high stored energy concentrated in deformation zones surrounding the particles further accelerates boundary migration, thereby enhancing subgrain growth and driving the completion of recrystallization [33].

This interpretation is further corroborated by the misorientation angle distribution profiles of AR and HT samples, illustrated in Figure 5. The fraction of HAGBs increased significantly in the HT

 doi:10.20944/preprints202509.2423.v1

sample compared to the AR sample, demonstrating the transformation of LAGBs into HAGBs through subgrain rotation and PSN-assisted nucleation during static recrystallization. The higher proportion of HAGBs in the HT specimen reflects the replacement of subgrain boundaries with fully developed high-angle boundaries, indicating extensive strain accommodation and lattice rearrangement. This is further reinforced by the bar chart in Figure 5(c), which presents the fraction of recrystallized grains in each sample, determined based on the grain orientation spread (GOS < 2°) criterion [34]. It is evident from the analysis that the HT sample contains a substantially higher proportion of recrystallized grains, while the fraction of non-recrystallized grains is significantly reduced compared to the AR condition. Such evolution demonstrates that elevated thermal exposure during annealing promotes recovery, subgrain coalescence, and PSN, thereby facilitating the formation of new strain-free grains. Although the LAGB-to-HAGB transition is more commonly reported in DRX, similar evolution can also occur during static recrystallization via subgrain rotation in conjunction with the PSN effect. The true stress-strain curves of the AR and HT samples of Mg-Al-Zn-Ca alloy are presented in Figure 6 (a). The HT sample exhibits higher elongation and ultimate tensile strength (UTS), whereas the AR sample retains a higher yield strength (YS). Specifically, the YS decreased from 263 MPa in the AR state to 187.4 MPa after homogenization, while the UTS slightly increased from ~332 MPa to ~338 MPa, as highlighted in the bar graphs in Figure 6b.

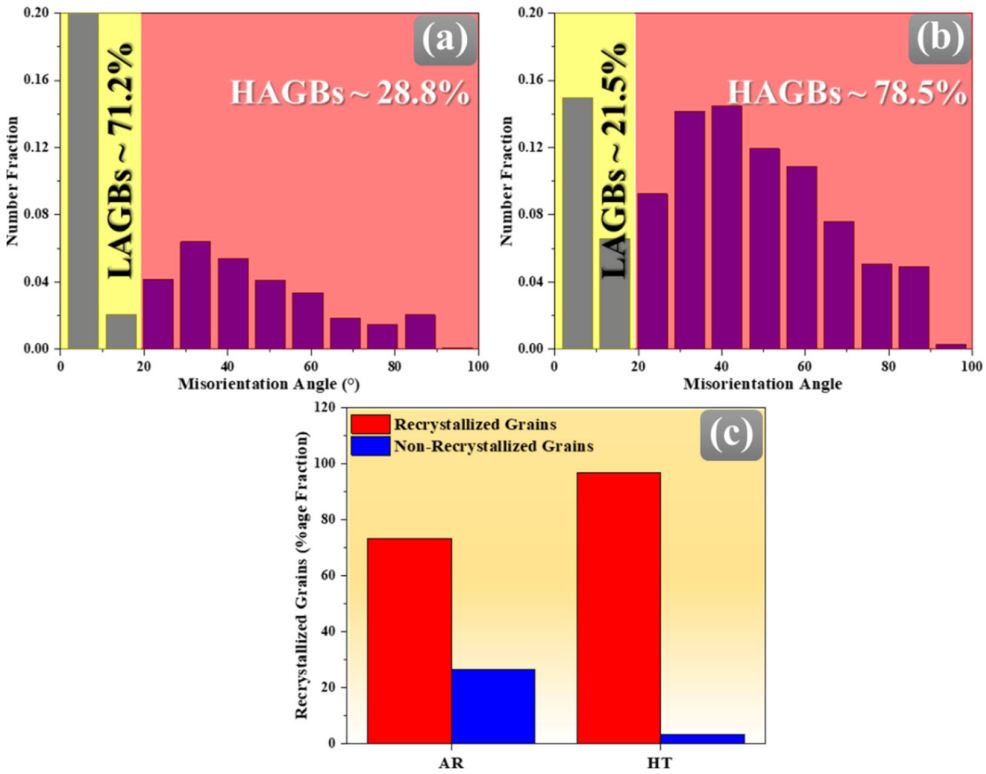

Figure 5. (a, b) Misorientation angle distribution profiles and **(c)** Bar chart showing variation in the fraction of recrystallized and non-recrystallized grains in AR and HT specimens of Mg-Al-Zn-Ca alloys, respectively.

 doi:10.20944/preprints202509.2423.v1

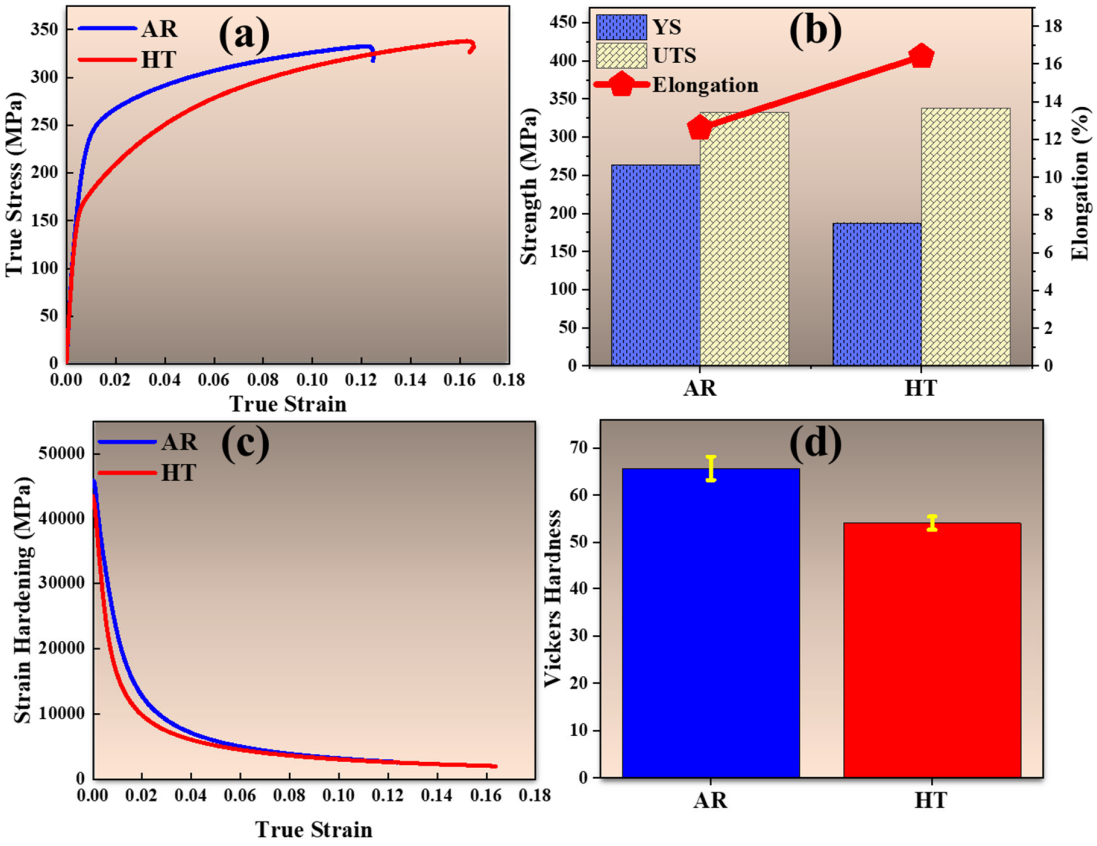

Figure 6. (a) True stress-strain curves, **(b)** Bar chart showing comparison of Strengths and Elongation, **(c)** Strain hardening behavior and **(d)** Vickers Hardness of AR and HT samples of Mg-Al-Zn-Ca alloys.

The elongation also improved significantly, increasing from 12.6% in the AR sample to 16.4% in the HT condition. The strain hardening rate curves in Figure 6c further show that the AR sample maintains a higher strain hardening rate throughout deformation, indicative of greater resistance to dislocation motion and enhanced strengthening during plastic flow. In contrast, the HT sample displays a reduced strain hardening rate, reflecting the microstructural softening and increased ease of dislocation movement following heat treatment. Similarly, the hardness results in Figure 6d reveal a decrease from 65.7 HV for the AR sample to 54.1 HV after homogenization, indicating overall softening associated with the heat treatment. This reduction in Vickers hardness is closely linked to the lower dislocation density and relaxation of residual stresses induced by recrystallization, which also accounts for the drop in YS.

The observed property changes are closely linked to the underlying microstructural evolution. Homogenization treatment triggered recrystallization [35], which was strongly facilitated by the PSN effect [36,37]. Second-phase particles acted as nucleation sites [38], leading to the development of finer, equiaxed grains compared to the elongated, strain-hardened grains characteristic of the AR condition [39]. The kinetics of recrystallization were governed by the nucleation of Al_2Ca precipitates, which in turn influenced the mechanical behavior [40]. This refined and more homogeneous microstructure reduced localized stress concentrations and provided additional pathways for dislocation motion, thereby improving the alloy's ability to sustain plastic deformation [41]. At the same time, the significant drop in YS and hardness can be attributed to the annihilation of dislocations and the relaxation of residual stresses during recrystallization, which lowered the resistance to plastic deformation [42]. Therefore, the mechanical response of the HT sample Mg-Al-Zn-Ca alloy reflects the combined effects of recrystallization-induced grain refinement and microstructural homogenization. While yield strength and hardness decreased due to dislocation annihilation and stress relaxation, the formation of fine, equiaxed grains and weakened texture enhanced ductility and

 doi:10.20944/preprints202509.2423.v1

slightly increased UTS. These changes highlight the critical role of recrystallization in balancing strength and plasticity, enabling simultaneous improvement in formability and overall mechanical performance.

4. Conclusions

This study demonstrates that homogenization treatment profoundly modifies the microstructure, texture, and mechanical performance of the Mg-3Al-1Zn-1Ca alloy through a complex interplay between recrystallization and precipitate-boundary interactions. The Al_2Ca exerted a dual influence by promoting recrystallization via PSN and restricting grain growth through Zener pinning. EBSD-based orientation analyses revealed that homogenization facilitated extensive recrystallization, reduced dislocation density, and converted low-angle boundaries into high-angle boundaries, thereby relieving internal stresses and refining the overall microstructure. Concurrently, texture analysis indicated the emergence of stronger basal components, accompanied by weaker secondary orientations introduced by PSN. Mechanically, homogenization led to a reduction in yield strength and hardness, reflecting the annihilation of dislocations and stress relaxation, while ultimate tensile strength remained nearly unaffected and ductility was significantly improved. This effectively demonstrates the role of post-annealing treatment in improving the formability of the hot-rolled alloy while retaining adequate load-bearing capacity.

Author Contributions: Conceptualization, A.R.K., H.M.R.T, U.M.C. and T.S.J.; methodology, H.M.R.T., M.I. and H.S.B.; software, H.M.R.T., H.S.B. and U.M. C.; validation, M.I. and U.M.C.; formal analysis, A.R.K., H.M.R.T, U.M. C. and M.I. X.X.; investigation, H.M.R.T. R.K.A. and H.S.B.; resources, T.S.J.; data curation, R.K.A., H.M.R.T , M.I. and U.M.C.; writing—original draft preparation, H.M.R.T.; writing—review and editing, R.K.A. and T.S.J.; supervision, T.S.J.; project administration, T.S.J.; funding acquisition, T.S.J. All authors have read and agreed to the published version of the manuscript.

Funding: This work was supported by Post-Doctoral Research Program for Excellence Institute (2024) in the Incheon National University.

Data Availability Statement: The original contributions presented in this study are included in the article. Further inquiries can be directed to the corresponding author.

Acknowledgments: This work was supported by Post-Doctoral Research Program for Excellence Institute (2024) in the Incheon National University.

Conflicts of Interest: The authors declare no conflicts of interest.

Abbreviations

The following abbreviations are used in this manuscript:

AR	As received
HT	Heat treated
IPF	Inverse pole figure
PSN	Particle simulated nucleation
EBSD	Electron back scattered diffraction
GOS	Grain orientation spread
KAM	Kernel average misorientation

References

1. Chaudry, U. M.; Farooq, A.; Sufyan, M.; Tariq, H. M. R.; Malik, A.; Kim, M.; Tariq, A.; Hamad, K.; Jun, T.-S., Corrosion behavior of AZ31 and AZ31-0.5 Ca in different concentrations of NaCl and Na2SO4 at various temperatures. *Corrosion* **2025,** 81, (3), 232-244.
2. Zhou, J.; Wu, M.; Zhang, W.; Ning, J., High-Temperature Deformation Behaviors of Gradient-Structured Mg-Gd-Y-Zr Alloys at High Strain Rates. *Materials* **2025,** 18, (17), 4085.

 doi:10.20944/preprints202509.2423.v1

3. Nidadavolu, E.; Mikulics, M.; Wolff, M.; Ebel, T.; Willumeit-Römer, R.; Zeller-Plumhoff, B.; Mayer, J.; Hardtdegen, H. H., Correlative Raman Spectroscopy–SEM Investigations of Sintered Magnesium–Calcium Alloys for Biomedical Applications. *Materials* **2025,** 18, (16), 3873.
4. Mukhtar, S.; Kamran, M.; Tayyeb, A.; Hussain, F.; Ishtiaq, M.; Riaz, F.; Asghar, W., Composition design and performance analysis of binary and ternary Mg-Zn-Ti alloys for biomedical implants. *Journal of Biological Physics* **2025,** 51, (1), 9.
5. Chaudry, U. M.; Tariq, H. M. R.; Ansari, N.; Kim, C.-S.; Lee, S. Y.; Jun, T.-S., Exceptional improvement in the yield strength of AZ61 magnesium alloy via cryo-stretching and its implications on the grain growth during annealing. *Journal of Alloys and Compounds* **2024,** 970, 172630.
6. Tariq, H. M. R.; Chaudry, U. M.; Kim, C.-S.; Jun, T.-S., Synergetic improvement in strength and ductility of AZX211 Mg alloy facilitated by {10–12}-{01–12} twin-twin interactions during pre-stretching at cryogenic temperature. *Journal of Materials Research and Technology* **2024**.
7. Hafiz Muhammad Rehan, T.; Umer Masood, C.; Jeong-Rim, L.; Nooruddin, A.; Mansoor, A.; Tea-Sung, J., Tensile Failure Mode Transitions from Subzero to Elevated Deformation Temperature in Mg-6Al-1Zn Alloy. *International Journal of Minerals, Metallurgy and Materials* **2025**.
8. Zhang, Z.; Kim, J.; Lee, T.; Li, M.; Gao, Y.; Pan, F., Effect of Substituting Y with Gd on LPSO Phase Dispersion and Mechanical Properties of Mg-2Ni-2Y Alloy. *Metals and Materials International* **2023**, 1-11.
9. Khan, M. A.; Afifi, M. A.; Hafeez, M. A.; Chaudry, U. M.; Brechtl, J.; Zulfiqar, M.; Tariq, H. M. R.; Hussain, M. A.; Kamran, M.; ishtiaq, M., Evolution of microstructure, texture, and mechanical performance of Mg-13Gd-2Er-0.3 Zr alloy by double extrusion at different temperatures. *Archives of Civil and Mechanical Engineering* **2024,** 25, (1), 26.
10. Chaudry, U. M.; Tariq, H. M. R.; Zubair, M.; Ansari, N.; Jun, T.-S., Implications of twinning on the microstructure development, crystallographic texture and mechanical performance of Mg alloys-a critical review. *Journal of Magnesium and Alloys* **2023,** 11, (11), 4146-4165.
11. Chaudry, U. M.; Rehan Tariq, H. M.; Hamad, K.; Khan, M. K.; Jun, T.-S., Twinning-induced texture weakening in Mg alloy and its consequent influence on ductility and formability. *Materials Science and Technology* **2025,** 41, (2), 101-105.
12. Zhou, W.; Aprilia, A.; Mark, C. K., Mechanisms of cracking in laser welding of magnesium alloy AZ91D. *Metals* **2021,** 11, (7), 1127.
13. Li, X.; Jiao, F.; Al-Samman, T.; Chowdhury, S. G., Influence of second-phase precipitates on the texture evolution of Mg–Al–Zn alloys during hot deformation. *Scripta Materialia* **2012,** 66, (3-4), 159-162.
14. Tariq, H. M. R.; Ishtiaq, M.; Kang, H.-H.; Chaudry, U. M.; Jun, T.-S., A Critical Review on the Comparative Assessment of Rare-Earth and Non-Rare-Earth Alloying in Magnesium Alloys. *Metals* **2025,** 15, (2), 128.
15. Tariq, H. M. R.; Chaudry, U. M.; Kim, C.-S.; Jun, T.-S., Synergetic improvement in strength and ductility of AZX211 Mg alloy facilitated by {10–12}-{01–12} twin-twin interactions during pre-stretching at cryogenic temperature. *Journal of Materials Research and Technology* **2024,** 29, 3249-3254.
16. Chaudry, U. M.; Tariq, H. M. R.; Ansari, N.; Mansoor, A.; Khan, M. K.; Hamad, K.; Jun, T.-S., Effect of CaO Content and Annealing Treatment on the Room-Temperature Mechanical Properties of AZ61 and AZ61-CaO Alloys. *Metals* **2023,** 13, (12), 1962.
17. Shah, S.; Liu, M.; Khan, A.; Ahmad, F.; Chaudry, U. M.; Khan, M. Y.; Abdullah, M.; Xu, S.; Peng, Z., Recrystallization aspects and factors affecting their roles in Mg alloys: A comprehensive review. *Journal of Magnesium and Alloys* **2025**.
18. Tariq, H. M. R.; Kang, H. H.; Chaudry, U. M.; Khan, M. K.; Jun, T. S., Impact of Surface Roughness on the Yield Drop of Hot-Rolled AZX311 Mg Alloy. *Advanced Engineering Materials* **2024**, 2401689.
19. Hussain, F.; Manzoor, M. U.; Kamran, M.; Ahmad, T.; Riaz, F.; Mukhtar, S.; Rehan Tariq, H. M.; Ishtiaq, M., Optimizing Biocompatibility of Mg-AZ31B Alloy through Varied Surface Roughness and Anodization Time. *Iranian Journal of Materials Science & Engineering* **2024,** 21, (3).
20. Park, J.; Kim, M.; Yoon, U.; Kim, W., Microstructures and mechanical properties of Mg–Al–Zn–Ca alloys fabricated by high frequency electromagnetic casting method. *Journal of materials science* **2009,** 44, (1), 47-54.
21. Gneiger, S.; Papenberg, N.; Mitsche, S.; Fehlbier, M., Manufacturing and processing of sheets using a Mg–Al–Ca–Zn–Y alloy for automotive applications. *Results in Engineering* **2024,** 21, 101700.

 doi:10.20944/preprints202509.2423.v1

22. Zhang, L.; Deng, K.-k.; Nie, K.-b.; Xu, F.-j.; Su, K.; Liang, W., Microstructures and mechanical properties of Mg–Al–Ca alloys affected by Ca/Al ratio. *Materials Science and Engineering: A* **2015,** 636, 279-288.
23. Jiang, Z.; Jiang, B.; Yang, H.; Yang, Q.; Dai, J.; Pan, F., Influence of the Al2Ca phase on microstructure and mechanical properties of Mg–Al–Ca alloys. *Journal of Alloys and Compounds* **2015,** 647, 357-363.
24. Fan, Y.; Zhu, G.; Park, J.-S.; Zhang, X.; Song, Z.; Wang, H.; Zeng, X.; Wang, L., The role of Ca on the microstructure and tensile properties of Mg-Al-Zn-Ca alloys. *Materialia* **2023,** 29, 101787.
25. Tariq, H. M. R.; Chaudry, U. M.; Kim, C.-S.; Jun, T.-S., Effect of Calcium on the Rate of Grain Boundary Migration in Pure Magnesium During Annealing. *Metals and Materials International* **2024**, 1-6.
26. Siddique, J. A.; Kim, B. H.; Rafiei, S.; Shah, A. W.; Song, R.; Ha, S.-H.; Yoon, Y. O.; Lim, H. K.; Kim, S. K., Role of dislocation density on the onset and intensity of stretcher strain marks in novel Al-Mg alloys with high Mg content. *Journal of Materials Research and Technology* **2025,** 35, 5552-5562.
27. Pei, R.; Zou, Y.; Wei, D.; Al-Samman, T., Grain boundary co-segregation in magnesium alloys with multiple substitutional elements. *Acta Materialia* **2021,** 208, 116749.
28. Kim, H. J.; Jin, S.-C.; Jung, J.-G.; Park, S. H., Influence of undissolved second-phase particles on dynamic recrystallization behavior of Mg–7Sn–1Al–1Zn alloy during low-and high-temperature extrusions. *Journal of Materials Science & Technology* **2021,** 71, 87-97.
29. Zhang, L.; Wu, X.; Zhang, X.; Yang, X.; Li, Y., Constitutive model and recrystallization mechanism of Mg-8.7 Gd-4.18 Y-0.42 Zr magnesium alloy during hot deformation. *Materials* **2022,** 15, (11), 3914.
30. Tariq, H. M. R.; Chaudry, U. M.; Suh, J. S.; Kim, Y. M.; Jun, T.-S., Effect of cryogenic temperature on the strengthening mechanisms of AZ61 Mg alloy extruded at different temperatures. *Journal of Materials Research and Technology* **2024,** 33, 335-348.
31. Zheng, C.; Chen, S.; Cheng, M.; Zhang, S.; Li, Y.; Yang, Y., Controlling dynamic recrystallization via modified LPSO phase morphology and distribution in Mg-Gd-Y-Zn-Zr alloy. *Journal of Magnesium and Alloys* **2023,** 11, (11), 4218-4234.
32. Tariq, H. M. R.; Chaudry, U. M.; Ishtiaq, M.; Kim, M.; Ali, M.; Jun, T.-S., Effect of Al addition on the room and cryogenic temperature deformation of Mg-xAl-1Zn-1Ca alloy (x= 1, 2 wt.%). *Journal of Magnesium and Alloys* **2024,** 12, (11), 4694-4708.
33. Zhu, G.; Wang, L.; Wang, J.; Wang, J.; Park, J.-S.; Zeng, X., Highly deformable Mg–Al–Ca alloy with Al2Ca precipitates. *Acta Mater.* **2020,** 200, 236-245.
34. Chaudry, U. M.; Lee, M.-S.; Jun, T.-S., Dynamic recrystallization of commercially pure titanium during cryogenic compression. *Materials Characterization* **2023,** 206, 113423.
35. Changizian, P.; Zarei-Hanzaki, A.; Abedi, H. R., On the recrystallization behavior of homogenized AZ81 magnesium alloy: The effect of mechanical twins and γ precipitates. *Materials Science and Engineering: A* **2012,** 558, 44-51.
36. Shah, S. S. A.; Liu, M.; Khan, A.; Ahmad, F.; Chaudry, U. M.; Khan, M. Y.; Abdullah, M. R.; Xu, S.; Peng, Z., Recrystallization aspects and factors affecting their roles in Mg alloys: A comprehensive review. *Journal of Magnesium and Alloys* **2025,** 13, (5), 1879-1914.
37. Robson, J. D.; Henry, D. T.; Davis, B., Particle effects on recrystallization in magnesium–manganese alloys: Particle-stimulated nucleation. *Acta Mater.* **2009,** 57, (9), 2739-2747.
38. Zhang, K.; Shao, Z.; Jiang, J., Effects of twin-twin interactions and deformation bands on the nucleation of recrystallization in AZ31 magnesium alloy. *Materials & Design* **2020,** 194, 108936.
39. Kim, H. J.; Jin, S.-C.; Jung, J.-G.; Park, S. H., Influence of undissolved second-phase particles on dynamic recrystallization behavior of Mg–7Sn–1Al–1Zn alloy during low- and high-temperature extrusions. *Journal of Materials Science & Technology* **2021,** 71, 87-97.
40. Masood Chaudry, U.; Hoo Kim, T.; Duck Park, S.; Sik Kim, Y.; Hamad, K.; Kim, J.-G., On the High Formability of AZ31-0.5Ca Magnesium Alloy. *Materials* **2018,** 11, (11), 2201.
41. Huang, K.; Logé, R. E., A review of dynamic recrystallization phenomena in metallic materials. *Materials & Design* **2016,** 111, 548-574.
42. Raabe, D., 23 - Recovery and Recrystallization: Phenomena, Physics, Models, Simulation. In *Physical Metallurgy (Fifth Edition)*, Laughlin, D. E.; Hono, K., Eds. Elsevier: Oxford, 2014; pp 2291-2397.

 doi:10.20944/preprints202509.2423.v1